

## Accepted (peer-reviewed) version

This document is the Accepted Manuscript version of a Published Work that appeared in final form in *Solar Energy Materials and Solar Cells*, Volume 241, 1 July 2022, 111760, Date of publication: Apr 2022, copyright © 2022 Elsevier B.V., after peer review and technical editing by the publisher.

To access the final edited and published work see:  
<https://doi.org/10.1016/j.solmat.2022.111760>

## Towards the scale-up of solid-state, low-emissive electrochromic films, fabricated on a single substrate with novel electrolyte formulations.

Alessandro Cannavale<sup>1,2\*</sup>, Marco Pugliese<sup>2</sup>, Roberto Giannuzzi<sup>3,\*</sup>, Riccardo Scarfiello<sup>2</sup>, Carmela Tania Prontera<sup>2</sup>, Vitantonio Primiceri<sup>2</sup>, Marco Mazzeo<sup>2,4</sup>, Francesco Martellotta<sup>1</sup>, Ubaldo Ayr<sup>1</sup>, Francesco Fiorito<sup>3</sup>, Fabrizio Mariano<sup>2</sup>, Antonio Maggiore<sup>2</sup>, Vincenzo Maiorano<sup>2</sup>, Giuseppe Gigli<sup>2</sup>.

<sup>1</sup>Department of Civil Engineering Sciences and Architecture, Polytechnic University of Bari, Bari, Italy

<sup>2</sup>National Research Council, Institute of Nanotechnology (CNR-NANOTEC), Via Monteroni, 73100 Lecce, Italy

<sup>3</sup>Department of Civil, Environmental, Land, Building Engineering and Chemistry, Polytechnic University of Bari, Bari, Italy

<sup>4</sup> Department of Mathematics and Physics "Ennio De Giorgi" - University of Salento- 73100 Lecce, Italy;

\*Corresponding Authors: [alessandro.cannavale@poliba.it](mailto:alessandro.cannavale@poliba.it), [roberto.giannuzzi@unisalento.it](mailto:roberto.giannuzzi@unisalento.it)

### Abstract

This experimental work reports the activities of design, fabrication and characterization of an innovative solid-state electrochromic device, deposited on a single substrate with high transparency in the bleached conditions and a wide modulation of transmittance ( $\Delta T$  of 60% at 750 nm) both in the visible and near-infrared wavelengths. A tailored formulation of the solid electrolytes, based on sulfonated tetrafluoroethylene-based fluoropolymer-copolymer dispersions and the accurate design of a suitable layer of porous tin oxide nanoparticles provided high coloration and bleaching kinetics and recovery of the pristine conditions, even after 500 complete cycles. Devices were scaled-up to 10x10 cm<sup>2</sup> size, without mechanical and aesthetic defects and relevant homogeneity, throughout the coloration and bleaching processes. Furthermore, this device shows the further feature to be a low-emissivity dynamic solar control film, highly compatible with integration within insulated glazed units.

### 1. Introduction

The rapid evolution of ongoing climate change and phenomena related to global warming has forced a rapid revision of the regulations relating to the construction sector, responsible for a very large amount of energy consumption on a global scale. According to the European Directive 2018/844, buildings contribute to 36% of greenhouse gas emissions; furthermore, about 50% of final energy consumption in the European Union is used for heating and cooling [1]. This roadmap requires the fast evolution of new technologies capable of producing energy (such as photovoltaics or solar-thermal [2–4]) or providing control and reduction of energy consumption. The so-called smart-windows belong to the latter type [5–9]. Typically, they embody chromogenic materials, which change their spectral properties according to the application of precise external stimuli. For example, thermochromic materials undergo a significant modulation in their transmittance spectrum upon reaching a critical temperature [10–13]; on the other hand, photo-chromic materials change their color in the presence of radiation of given wavelengths [14–16]; finally, electro-chromic (EC) devices undergo a chromatic transition as a consequence of a small electric potential, applied by means of an external circuitry [17–21]. Building integration of smart windows allows for a variety of benefits. As well known, windows constitute a point of thermal weakness in the envelope, which results in an increase in thermal loads for air conditioning in summer (or in winter), depending on the location [22,23]. In hot climates, windows allow the penetration of undesired thermal loads, which result in a conspicuous increase of energy expenditure for air conditioning [24,25]. In fact, glazing used in architecture offers a significant transparency to solar radiation (250–2500 nm) but, at the same time, it is opaque to radiation with a longer wavelength, due to the intrinsic glass properties. The thermal radiation trapped in the internal space results in a "greenhouse effect", due to excess accumulated thermal load. Smart windows dynamically modulate the spectral properties of a glass, allowing users to reduce - even drastically - the flow of radiation that penetrates through the glazed components. This modulation - which can be expressed by means of the so-called solar heat gain coefficient (SHGC), otherwise termed as solar factor (g-factor) - can affect both visible and infrared radiation to a greater or lesser extent. Several studies have calculated, by means of numerical simulations or experimental campaigns, the achievable reduction in energy consumption for air conditioning with very convincing results [26–29]. It was also noted that smart windows can also offer benefits in terms of visual comfort for the occupants [30,31]. The reduction of the optical transmittance of the glass, in the presence of excess solar radiation, in fact, offers a useful shielding with the benefit of maintaining a beneficial visual interaction with the external environment; furthermore, phenomena of visual discomfort for the occupants are significantly reduced. This reduction was assessed adopting various metrics, commonly used in the field of natural lighting, such as the Useful Daylight Illuminance, Daylight Glare Probability or Daylight Glare Index [32–34]. Among the wide class of chromogenics, EC devices typically feature a 5-layer architecture that closely resembles an electrochemical battery. They work in an "active" fashion and for this reason can be a suitable for integration in buildings: users can activate or even override them, according to their needs. EC devices generally embody two transparent substrates, made conductive by depositing thin films of conductive transparent oxides (such as FTO or ITO), two layers of EC materials with complementary functionality (i.e. EC materials with anodic and cathodic behaviour, such as tungsten trioxide ( $\text{WO}_3$ ) and oxide nickel (NiO)) and finally an interposed electrolyte [35]. The electrolyte layer has the function of conducting ions inside the device, following the application of a DC bias; on the other hand, the mobility of electrical charges is entrusted to an external circuitry. The fundamental role of electrolytes in the technological evolution of EC devices is undeniable [36–

38]. While on the one hand EC devices containing liquid electrolytes have optimal kinetics, due to their higher ion conductivity, on the other hand it must be taken into account that they are subject to leakage, due to insufficient sealing of the device, evaporation of solvents, stability [39]. In the last few decades, a lot of effort has been made to design gel or completely solid electrolytes to face these open issues and increase the durability of smart windows. As expected, the main difficulty in the design of solid-state electrolytes is to ensure a high ionic mobility, despite the use of a material in a solid state of aggregation [40]. In recent years, a considerable boost has been given to research on devices containing solid-state electrolytes, based on organic or inorganic materials [41,42]. Solid-state EC devices embodying inorganic materials were reported by Niwa et al. [43], who used solid electrolytes made of tantalum oxide. Chen et al. [44] adopted LiF solid electrolytes deposited by resistance evaporation, obtaining very fast response and large optical contrast. Such EC devices were based on the simple architecture glass/ITO/WO<sub>3</sub>/LiF/NiO/ITO. EC devices by Zhu et al. [45] were based on the use of Li<sub>x</sub>NiO<sub>y</sub> films. Li et al. [46] reported all solid state EC devices with high durability, achieved by tuning the annealing process in the fabrication process of devices with a glass/ITO/NiO/ ZrO<sub>2</sub>/Li/WO<sub>3</sub>/ITO architecture. They observed superior stability in EC devices annealed at 400 °C, even after 50000 cycles. A review dealing with inorganic EC devices has been provided by Patel et al. [47].

In this work, a large area solid state EC device is reported, with a simplified architecture, fabricated at room temperature. The device proposed hereafter was designed to combine simplification and stability, compared to previously reported architectures: novel electrolyte solutions were studied, and a suitable layer devoted to ion storage was adopted, made of tin oxide nanoparticles. Furthermore, this device allows to reduce process costs (being deposited on a single substrate) and - at the same time - offers the further feature of operating as a low-emissivity dynamic solar control film, highly compatible with integration in insulated glazed units.

## 2. Methodology

### 2.1 Fabrication of EC devices

Tin doped indium tin oxide (In<sub>2</sub>O<sub>3</sub>:SnO<sub>2</sub>)-coated glass substrates (2.5 cm x 2.5 cm, with sheet resistance of 12 Ω/sq) were cleaned in a detergent solution using an ultrasonic bath for 10 min, and then washed with acetone and 2-propanol. Once the substrates were completely cleaned, a liquid solution of Tin Oxide (Tin(IV) Oxide, 15% in H<sub>2</sub>O colloidal dispersion - SnO<sub>2</sub> by Alfa Aesar, having an average size of 15÷20 nm) was deposited on half of previously prepared substrates, by spin-coating at 2000 rpm for 60 s. Afterwards, they were annealed at 250 °C for 30 minutes. Substrates coated with SnO<sub>2</sub> solution, acting as an ion storage layer, were named as "S", whereas those with only ITO were named "I". Scanning electron microscopy (SEM) images of the SnO<sub>2</sub> layers deposited on top of In<sub>2</sub>O<sub>3</sub>:SnO<sub>2</sub> substrates and the cross section are reported in Supporting Information (Figure S1). The thickness of such layers was about 70 nm. SEM images were acquired by means of a FEI Nova NanoSEM 200 microscope field emission gun (accelerating voltage of 5 kV). Nafion and Lithion solutions in 2-propanol alcoholic solvents (from Ion Power, GmbH, Germany) were used to prepare two electrolyte solutions (called A and B, respectively), using different amounts, derived from previous experimental optimization. More in detail, several formulations were tested in laboratory scale devices, starting from electrolytes containing only Lithion and only Nafion. The first

ones showed a typical yellowish color and this represents a limit for aesthetic reasons. Transmittance spectra of all the electrolytes are reported in Figure S3. On the other hand, electrolytes containing only Nafion, if scaled-up, underwent severe cracking. For this reason, mixed solutions were investigated. Solutions formulated with excess Nafion reported several cracks and were soon abandoned. Better performances were obtained using electrolytes containing 60% (or 70%) of Lithion and containing Nafion, for the remainder. More in detail, the best performing electrolytes were “A-electrolyte”, that was prepared by mixing 40% wt of Nafion solution and 60% wt of Lithion, whereas “B-electrolyte” contains 30% wt of Nafion solution and 70% wt of Lithion. After stirring the two electrolytes for at least 24 hours at room temperature, they were diluted with 2-propanol (10% wt). Electrolytes were then sonicated for 20 minutes before being deposited by spin-coating at 600 rpm for 60s and then dried at room temperature in ambient air. The thickness of deposited films was measured by means of a profilometer (VeecoDektak6M) and ranged from 7  $\mu\text{m}$  to 8  $\mu\text{m}$ . A thin film (300 nm) of tungsten oxide ( $\text{WO}_3$ ) was deposited by thermal evaporation, with a pressure of  $3.6 \cdot 10^{-5}$  mbar and a deposition rate of 1.0  $\text{\AA}/\text{s}$ . An  $\text{In}_2\text{O}_3:\text{SnO}_2$  electrode layer was deposited by RF-sputtering onto the devices, in high vacuum conditions ( $3 \cdot 10^{-3}$  mbar) with a power of 75 W at room temperature (the Argon flux was set at 10 sccm). The process was completed when films reached a thickness of 300 nm. Sheet resistance of these layers deposited on top of the electrolytes was about  $20 \Omega/\square$ . Its properties influence both the optical transmittance and the electrical properties of the devices. A cross-sectional view of the device and an axonometric diagram are reported in **Figure 1**.



**Figure 1** – Cross-sectional view of the device (left side) and axonometric diagram (right side) reporting all the layers deposited.

The devices were fabricated using the two electrolytes prepared, A and B. Moreover, both of the electrolytes were employed to fabricate both devices embodying  $\text{SnO}_2$  (acting as ion storage layer, for AS and BS devices) and devices without the storage layer (named AI and BI). All the structures of devices studied in this work are summarized in **Table 1**.

Table 1 – Structure of devices AI, AS, BI, BS.

Device name	Device AI	Device AS	Device BI	Device BS
Transparent conductive oxide	ITO:SnO <sub>2</sub>	ITO:SnO <sub>2</sub>	ITO:SnO <sub>2</sub>	ITO:SnO <sub>2</sub>

Electrochromic material	WO <sub>3</sub>	WO <sub>3</sub>	WO <sub>3</sub>	WO <sub>3</sub>
Electrolyte	Electrolyte A	Electrolyte A	Electrolyte B	Electrolyte B
Ion storage layer	/	SnO <sub>2</sub> nanoparticles	/	SnO <sub>2</sub> nanoparticles
Transparent conductive oxide	ITO:SnO <sub>2</sub>	ITO:SnO <sub>2</sub>	ITO:SnO <sub>2</sub>	ITO:SnO <sub>2</sub>
Substrate	Glass	Glass	Glass	Glass

## 2.2 Optical measurements

Transmittance spectra of the devices were measured on a Varian Cary 5000 UV-vis-NIR spectrophotometer in a wavelength range between 250 nm and 2200 nm after allowing for 300 s stabilization of the optical signal. Optical transmittance (T) and reflectance (R) spectra of the films were performed with a Varian Cary 5000 spectrophotometer equipped with an integrating sphere. Data collected were used to calculate visible transmittance ( $T_{vis}$ ), solar transmittance ( $T_{sol}$ ), visible reflectance ( $R_{vis}$ ) and solar reflectance ( $R_{sol}$ ), according to current technical standards [48]. Coloration and bleaching of Devices were obtained by applying external voltages (2.6 V and 0.7 V, respectively) by means of a Keithley Sourcemeter 2420.

## 2.3 Fourier Transform Infrared Spectroscopy (FT-IR)

FT-IR spectra were recorded over the 4000–400 cm<sup>-1</sup> wavenumber range at a resolution of 4 cm<sup>-1</sup> using a DairyGuard Milk Powder Analyzer spectrometer equipped with Reflectance Accessory. The bare silicon wafer was used for baseline correction.

## 2.4 Electrochemical measurements

Chronoamperometry measurements were performed on an AUTOLAB PGSTAT302N potentiostat in a two-electrode configuration, with an applied potential of +0.7 V and -2.6 V for the AI and AS devices. Coloration/bleaching kinetics were measured in-situ at 550 nm, with a potential switched between -2.6 V and +0.7 V for a 450 s holding time. Coloration efficiency was calculated from the slope of the optical density as a function of the charge density. Cyclic voltammetry was performed to assess the stability of devices, using the same instrument, in a voltage range between -2.6 V and +0.7 V, adopting a 5 mV/s scan rate.

In order to determine the ionic conductivity, electrolytes solutions were sandwiched between two round steel plates. After seven days, to allow for a complete evaporation of solvents, ionic conductivity was measured by means of electrochemical impedance spectroscopy, performed using the same potentiostat. The measurements were carried out at steady-state conditions by applying an AC voltage of 0.01 V in a frequency range spanning from 1 MHz to 0.1 Hz.

## 2.5 Calculation of emissivity

Normal emissivity has been calculated, starting from spectral data, according to the following expression:

$$\varepsilon_n = 1 - R_n = 1 - \frac{1}{30} \sum_{i=1}^{30} R_n(\lambda_i)$$

Where  $R_n$  represents average spectral reflectance calculated by summation of spectral reflectance values at 30 distinct wavelength ( $\lambda_i$ ) values from a table according to the regulation ISO 10292:1994, as reported in [21].

### 3. Results and Discussion

#### 3.1 Transmittance spectra and kinetics

Monochromatic transmittance values of devices are reported in **Figure 2**. All the spectra, plotted from 0.25  $\mu\text{m}$  to 2.2  $\mu\text{m}$ , show very similar properties, both in the bleached and in the coloured conditions. All of them show high transparency in the bleached state (which is higher than 80% in a wide range of frequencies throughout the visible spectrum), demonstrating that this device architecture may be suitable for integration within multiple insulated glazed units.

Optical properties of devices were quite similar, as testified by Figure S3, due to the slight transmittance differences observed between electrolytes A and B. The limited change of electrolyte formulations did not significantly affect their appearance. Apart from some small differences, the shape of spectra can be considered roughly superimposable. More in detail, AI device reported transmittance modulations of 42.0%, 59.1% and 50.2% at 600 nm, 750 nm and 1000 nm, respectively; similarly, AS devices reported modulations of 47.0%, 63.51% and 51%, measured at the same wavelengths. Such values confirm that the thin  $\text{SnO}_2$  layer - used as ion storage film - did not reduce dramatically transmittance as other aspects did (such as thickness, viscosity, and density of the electrolytes). The comparison between devices BI and BS showed similar figures and trends. BI device showed transmittance values of 42.2%, 59.3% and 49.41% at 600 nm, 750 nm and 1000 nm, whereas values observed in BS device were 43.5%, 59.7% and 47.5%.

The electrical properties of electrolytes are also quite similar, although those containing a higher percentage of Nafion were found to be more conductive. Ionic conductivity of Electrolyte A and Electrolyte B were in fact  $2.55 \cdot 10^{-3} \text{ S} \cdot \text{cm}^{-1}$  and  $1.88 \cdot 10^{-3} \text{ S} \cdot \text{cm}^{-1}$ , respectively.

On the other hand, transmittance in the coloured conditions exceeded 20% throughout the range of wavelengths considered. This is due to the absence of a complementary anodic EC material, working simultaneously in the coloration process and increasing the contrast. Higher bias may assure higher intercalation, but this may be obtained at the expenses of red/ox reversibility and durability of devices, which was one of the main targets of this experimental activity.

Graphs reported in **Figure 2** also plot a third family of curves, representing the bleached spectrum after at least 100 full cycles of coloration/bleaching. As it can be observed, the pristine properties of devices are fully recovered, especially in the visible range of wavelengths.

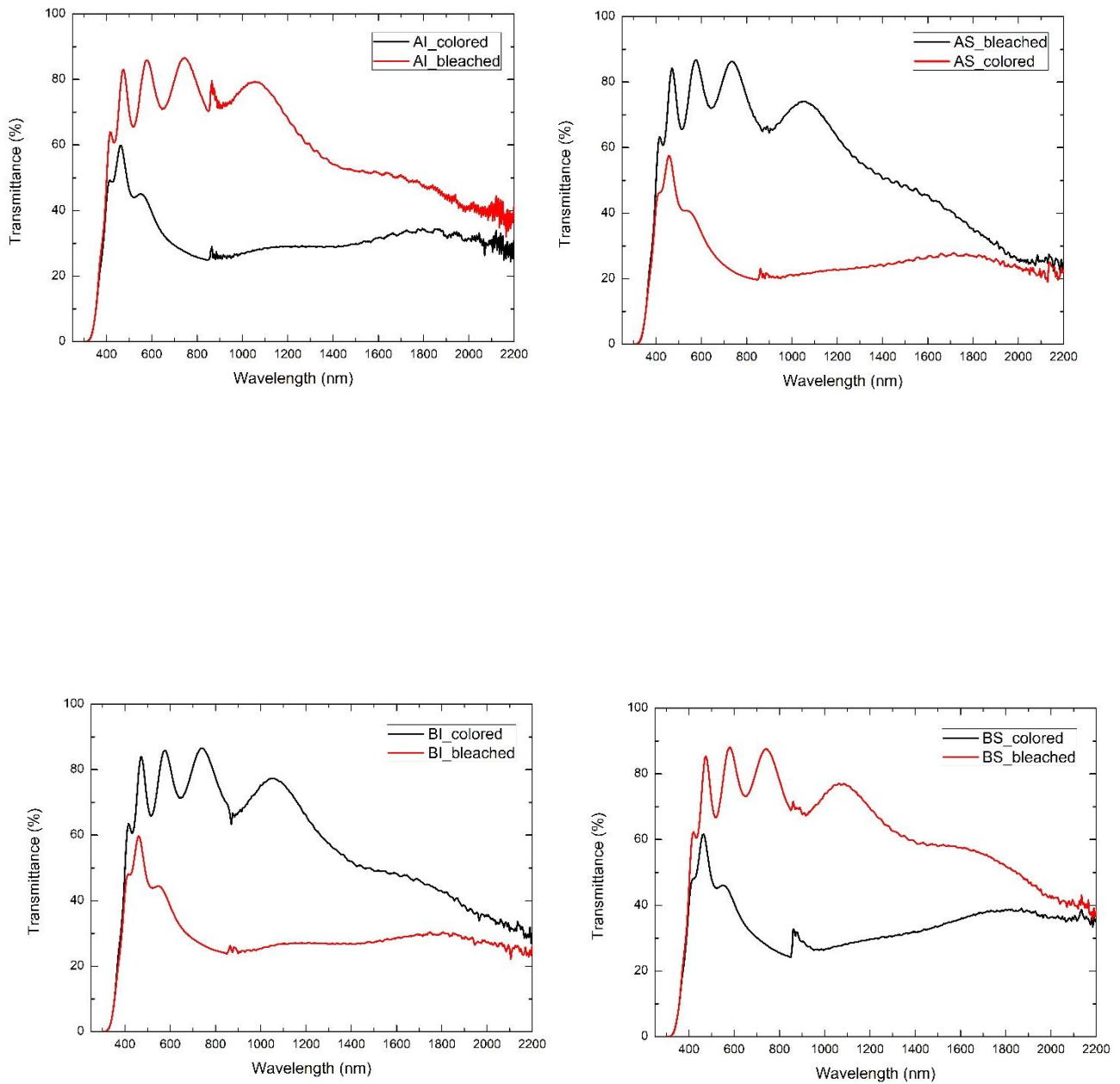


**Figure 2** – Transmittance spectra of devices AI, AS, BI and BS. (The irregular values observed in graphs at 800 nm are due to the grating change of the spectrophotometer).

Peaks and valleys observed in the shape of the bleached spectrum of devices are due optical interference due to the thickness of  $\text{WO}_3$  layers, as observed elsewhere [49]. Furthermore, the optical properties of the entire device are not affected by tin oxide and electrolyte layers; the ITO layer, on the other hand, mainly affects the NIR region of the graph, due to surface plasmon oscillation effect resulting in lower transmittance value in such spectral region.

The transmittance modulation observed in the four devices, between the coloured and bleached conditions is reported in **Figure 3**. The highest values were observed in the region of red and near

infrared wavelengths, due to the typical absorptive properties of amorphous tungsten trioxide ( $\text{WO}_3$ ). Maximum transmittance modulations exceeded 63% at 740 nm and were higher than 40% from 660 nm to 1200 nm for all the devices.

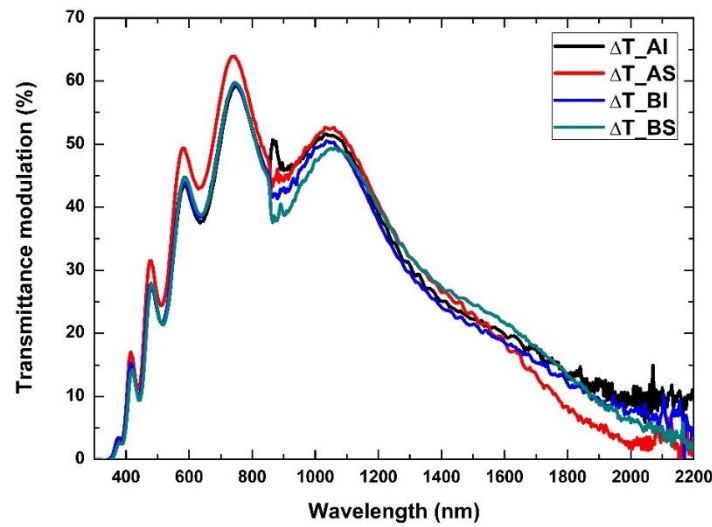


**Figure 3** – Transmittance modulation of devices.

### 3.2 Electric measurements and memory effect

The memory effect was measured for all the devices and the evolution of transmittance in time was plotted in **Figure 4**, keeping the devices in open-circuit conditions, after full coloration took place. After the first 2000 s, trends are clearly visible. Discharge trends are similar in devices AI and BI, due to the absence of an ion storage layer; in fact, device BS shows a different trend, with a faster discharge process. The nanoparticle  $\text{SnO}_2$  layer acts as a storage layer devoted to diffusion of cations, facilitating the bleaching process. On the other hand, Device AS starts from a lower value of transmittance but reports an intermediate trend, with respect to the two groups of devices. If on the one hand device BS recovers almost all the original transparency, after the time taken into consideration for the measurement (5 hours), device AS modulates only between 40% and 60%. Devices AI, AS and BI show a coloration loss lower than 25%, in open circuit mode. On the contrary, the change observed in Device BS exceeds 45%. Lower performance in terms of memory effect could lead to higher energy consumption of smart windows during their use. The different behaviour observed in Device AS is attributable to the higher amount of hydrogen ions in the electrolyte A, (which contains a higher amount of Nafion). Their reduced stoichiometric size favours their deeper cation intercalation, slowing down the bleaching process. On the contrary, the higher concentration of Lithion used in “B” electrolytes is associated to a greater concentration of lithium cations within the solution, with lower mobility within the structure of  $\text{WO}_3$ . Such ions, being wider than hydrogen ions, tend to intercalate less deeply (at the same voltage) and, probably, they de-intercalate more easily than hydrogen cations, in open-circuit conditions.

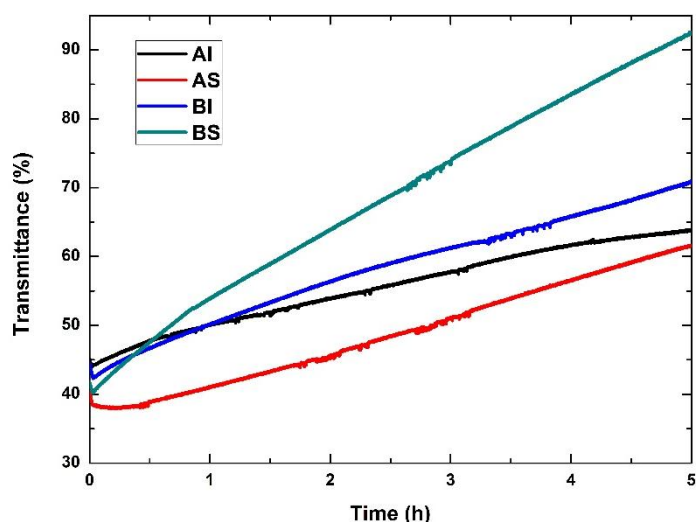


**Figure 4** – Spontaneous bleaching observed in open-circuit conditions (Data were collected at a wavelength of 600 nm).

**Figure 5a** show the chronoamperometric measurement of the AS and AI devices. As can be seen from **Figure 5a**, the chrono-amperograms completely overlap during the charging phase, while during the discharge process the AS device has a higher discharge current than AI one. **Figure 5b** and **Figure 5c** show the intercalated and deintercalated charge, calculated by integrating the current from the chronoamperometric measurements. The graph reveals that during the charging phase the two devices stored the same amount of charge, with comparable kinetics. However, during the discharge process, AS device was able to deintercalate more charge and faster than the AI device. This behaviour is related to the presence of the SnO<sub>2</sub> at the counter electrode, that allows more charge to be intercalated thanks to its higher surface area and to the intercalation properties of SnO<sub>2</sub>. This behaviour is mirrored by the coloration/bleaching kinetics of the two devices. The switching speed has been quantitatively assessed by monitoring *in-situ* the variation of the optical transmittance at 550 nm during the chronoamperometric test. Data are plotted in **Figure 5d,e**. Coloration time  $\tau_c$  (which has to be defined as the time to get a 90% of the maximum  $\Delta T$ ) has been estimated to be 257 s and 269 s, for AI and AS, respectively. However, the bleaching process of the AS device is faster than that of the AI device, requiring 18 s and 88 s respectively. This can be correlated to the presence of the SnO<sub>2</sub>. Moreover, one of the most useful parameters for evaluating the quality of an EC material or device is coloration efficiency (CE). A high CE can provide large optical modulation with small changes in insertion or extraction quantities and is a crucial parameter for practical devices because long-term cycling stability is enhanced by using lower charge insertion or extraction. CE can be extrapolated from the slope of the first linear region: it was estimated to lay around 69 cm<sup>2</sup>·C<sup>-1</sup> for AS device and 60 cm<sup>2</sup>·C<sup>-1</sup> for AI device.

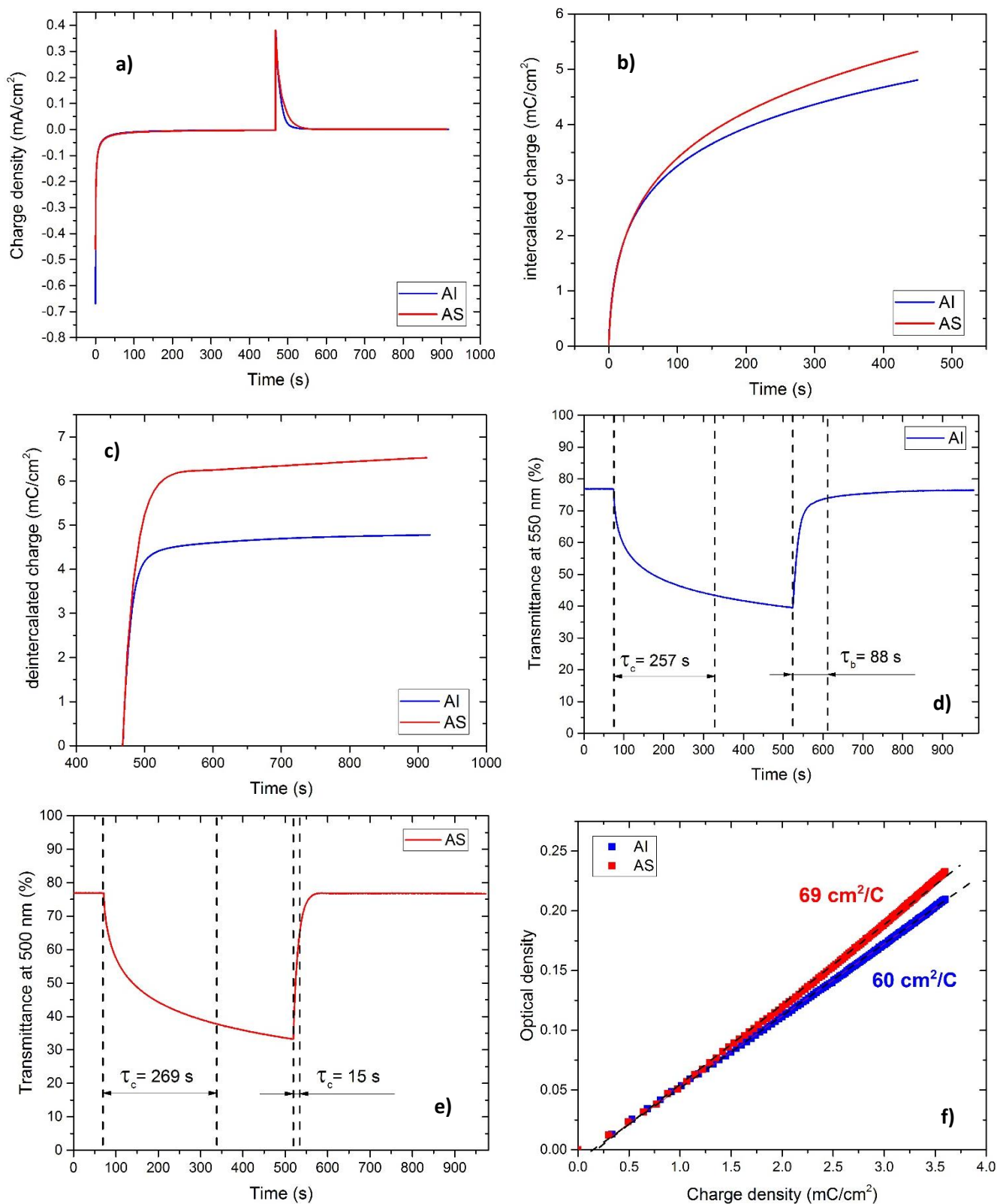


**Figure 5** – EC characterization of the AI (blue) and AS (red) device. (a) chrono-amperogram of the two devices obtained by applying a square wave voltage of 0.7 V/–2.6 V for 450 s. (b – c) Charge density of the cations intercalated and deintercalated, evaluated from chronoamperometric plots

(d - e) corresponding in-situ transmittance variation curve monitored at the wavelengths of 550 nm. (f) plot of optical density variation as a function of charge density monitored at 550 nm.

The stability of the AS device was investigated by means of cyclic voltammetry, performing 500 colouring/bleaching cycles. The device was cycled between  $-2.6$  V and  $+0.7$  V with  $5$  mV/s scan rate (Figure 6, left). After 500 cycles, the charging current (negative current) appears unaffected, whereas the discharge current (positive current) was reduced by about 11%. Consequently, the transmittance in the bleached (and in the colored state) was reduced by 5% over the entire wavelength range (Figure 6, right). However, after the stability test the AS device reported neither clear signs of degradation nor the presence of bubbles.

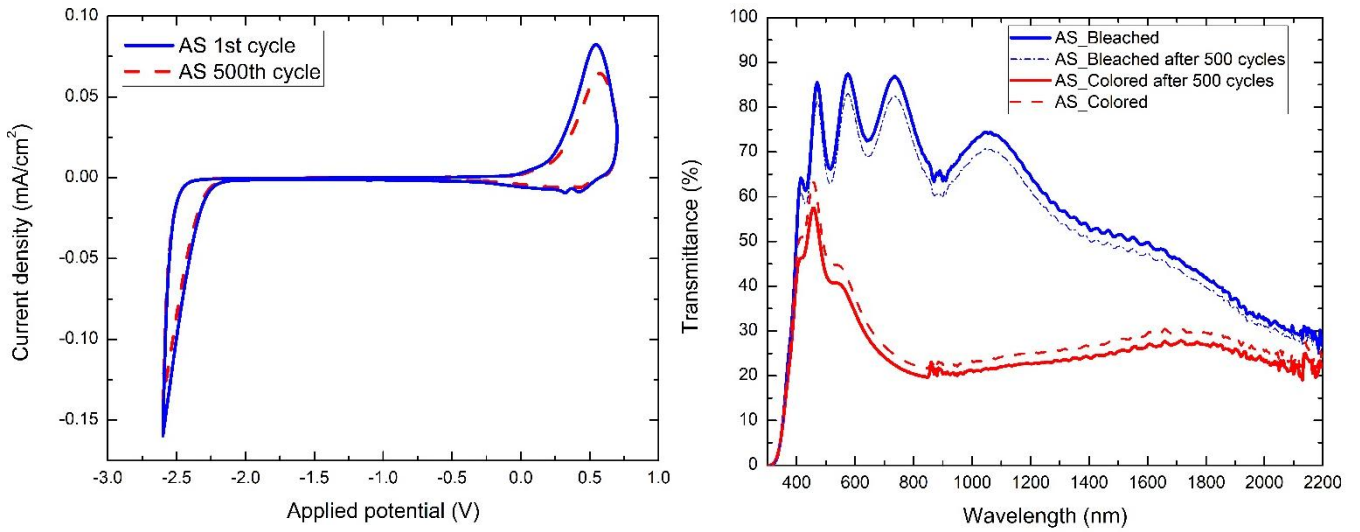


**Figure 6** – Cyclic voltammetry of Device AS, before and after 500 full cycles (Left) and respective transmittance spectra, between 300 nm and 2200 nm (Right).

### 3.3 Low-emissive properties and thermal performance

Reflectance spectra of ITO counter electrodes are reported in **Figure 7**, both in the solar range of wavelengths and in the infrared range. These data are consistent with the typical reflective properties of ITO. The value of normal emissivity ( $\epsilon_n$ ) obtained was 0.50. The corrected emissivity was then calculated, adopting a suitable correction coefficient ( $c_{CORR}$ ).

$$\epsilon = c_{CORR} \cdot \epsilon_n = \frac{\epsilon}{\epsilon_n} \cdot \epsilon_n$$

Such coefficient was determined by interpolating two values in the table reported in [21]. The value was then  $c_{CORR} = 1.03$ . Starting from measured spectra, the calculated value of emissivity of ITO surfaces was  $\epsilon = 0.52$ . Such value is lower than typical emissivity of glass (0.84) and it is compatible with values observed in literature for ITO coatings. Consequently, the proposed EC film may enhance thermal insulation properties, by reducing heat transfer in insulated glazed units (IGUs). Furthermore, all data reported in this work were collected without sealing our devices. The fluctuations in atmospheric moisture within our laboratory (HR typically ranging from 40% to 70%) did not affect performance in a dramatic way. This aspect could be relevant in view of an exploitation

of lower emissivity observed in devices, that could be integrated in the face 2 of IGUs for solar control and thermal purposes.

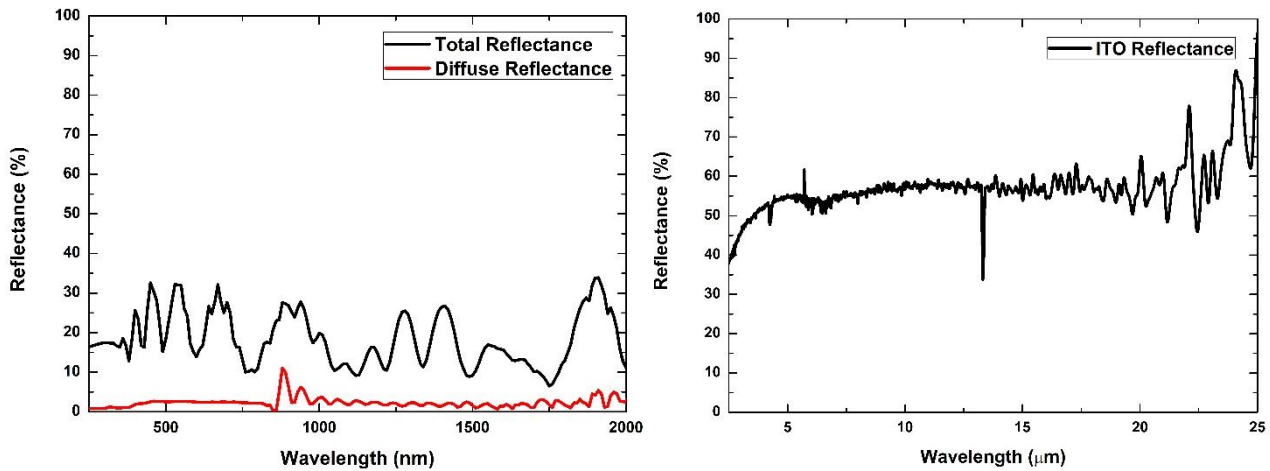


**Figure 7** – Total and diffuse reflectance (a) of Device AS, measures with a spectrophotometer; for the same device, absorbance and transmittance (b) measured with FTIR apparatus.

Furthermore, values of total and diffuse reflectance in the visible and solar range of wavelengths are pivotal to determine spectral properties of the here proposed EC devices. Such properties were calculated according to current technical standards and reported in **Table 2**, concerning only the best performing device (AS).

**Table 2** – Thermal and optical properties of Device AS in bleached and colored conditions ( $\epsilon_f$  and  $\epsilon_b$  represent the emissivity of front and back surface of glazing, respectively).

Device state	$T_{vis}$	$T_{sol}$	$R_{fvis}$	$R_{bvis}$	$R_{fsol}$	$R_{bsol}$	$\epsilon_f$	$\epsilon_b$	SHGC
AS bleached	0.77	0.67	0.08	0.24	0.08	0.20	0.84	0.52	0.73
AS colored	0.26	0.25	0.08	0.24	0.08	0.20	0.84	0.52	0.39

Furthermore, the present work involved the scale-up of the devices to obtain square prototypes, with a side of 10 cm, on a single glass substrate, shown in **Figure 8**. Devices did not undergo loss of performance if exposed to the external environment, during the experimental campaign, but a proper sealing of devices may improve their durability.

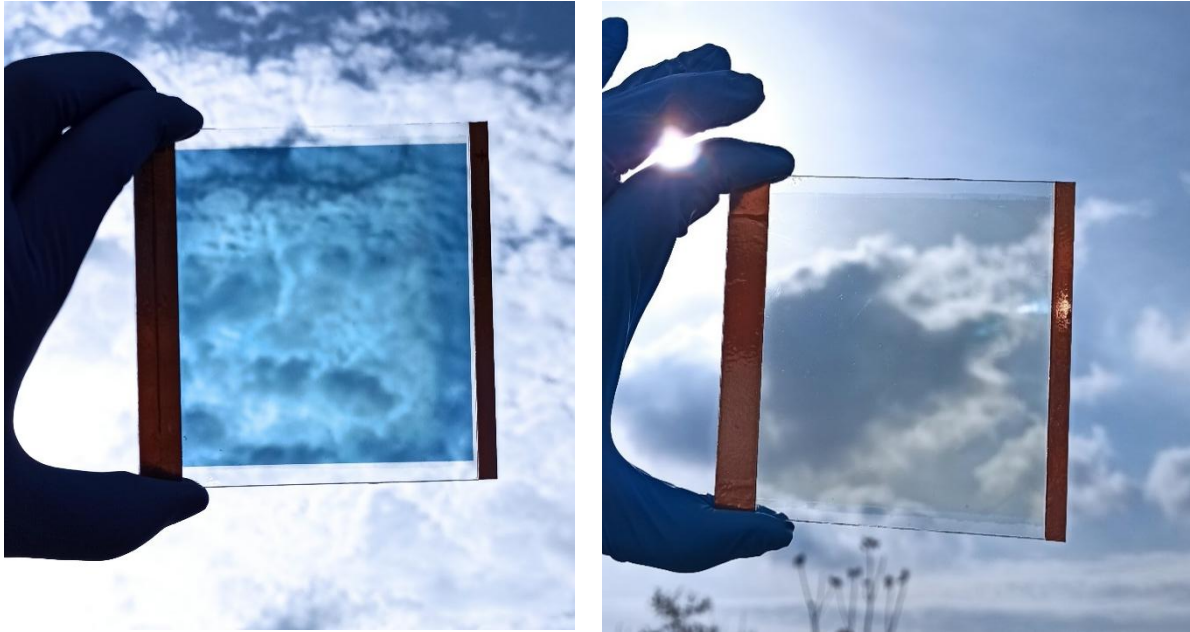


**Figure 8** – Scaled-up prototypes of solid-state EC devices, deposited on a single substrate in the bleached and colored conditions.

## Conclusion

In this experimental activity, the scale-up of EC smart window prototypes has been reported, with simplified architecture, high transparency in the bleached state (higher than 80% in the visible range) and high transmittance modulation in the visible (more than 60% at 700 nm) and infrared (about 50% at 1100 nm) ranges of the solar radiation. The detected coloration/bleaching processes are quite fast, compared with other solid-state devices (250 s for full coloration and 90 s for complete bleaching), despite the use of solid-state electrolyte formulations, containing Nafion and Lithion. An interesting low-emissivity characteristic ( $\epsilon = 0.52$ ) of the ITO layer was found, which could favour the control of radiative thermal exchange and the integration of the device in architectural windows.

## Acknowledgement

UA, AC, FM, MM kindly acknowledge Ministero dell'Università e della Ricerca for supporting their research activities through the program “Project PON ARS01\_01137 SE4I - Smart Energy Efficiency & Environment for Industry”.

## References

- [1] EU Parliament, Directive (EU) 2018/844 of the European Parliament and of the Council of 30 May 2018 Amending Directive 2010/31/EU on the Energy Performance of Buildings and Directive 2012/27/EU on Energy Efficiency, 2018. <https://eur-lex.europa.eu/eli/dir/2018/844/oj>.
- [2] S. Abdul Hamid, M. Yusof Othman, K. Sopian, S.H. Zaidi, An overview of photovoltaic thermal combination (PV/T combi) technology, *Renew. Sustain. Energy Rev.* 38 (2014) 212–222. doi:10.1016/j.rser.2014.05.083.

- [3] Y.T. Chae, J. Kim, H. Park, B. Shin, Building energy performance evaluation of building integrated photovoltaic (BIPV) window with semi-transparent solar cells, *Appl. Energy*. 129 (2014) 217–227. doi:10.1016/j.apenergy.2014.04.106.
- [4] S. Yang, A. Cannavale, D. Prasad, A. Sproul, F. Fiorito, Numerical simulation study of BIPV/T double-skin facade for various climate zones in Australia: Effects on indoor thermal comfort, *Build. Simul.* 12 (2019). doi:10.1007/s12273-018-0489-x.
- [5] C.G. Granqvist, Electrochromics and Thermochromics: Towards a New Paradigm for Energy Efficient Buildings, *Mater. Today Proc.* 3 (2016) S2–S11. doi:10.1016/j.matpr.2016.01.002.
- [6] A. Cannavale, U. Ayr, F. Fiorito, F. Martellotta, Smart electrochromic windows to enhance building energy efficiency and visual comfort, *Energies*. 13 (2020) 1–17. doi:10.3390/en13061449.
- [7] A. Piccolo, F. Simone, Energy performance of an all solid state electrochromic prototype for smart window applications, *Energy Procedia*. 78 (2015) 110–115. doi:10.1016/j.egypro.2015.11.123.
- [8] C.G. Granqvist, Oxide electrochromics: An introduction to devices and materials, *Sol. Energy Mater. Sol. Cells*. 99 (2012) 1–13. doi:10.1016/j.solmat.2011.08.021.
- [9] M. Hočevár, U. Opara Krašovec, A photochromic single glass pane, *Sol. Energy Mater. Sol. Cells*. 186 (2018) 111–114. doi:10.1016/j.solmat.2018.06.035.
- [10] M. Aburas, V. Soebarto, T. Williamson, R. Liang, H. Ebendorff-Heidepriem, Y. Wu, Thermochromic smart window technologies for building application: A review, *Appl. Energy*. 255 (2019) 113522. doi:10.1016/j.apenergy.2019.113522.
- [11] X. Ma, S. Zhao, L. Wang, H.J. Zhou, Research on the behaviors of extending thermo-chromic colors for a new thermo-chromic microcapsule, *J. Text. Inst.* 111 (2020) 1097–1105. doi:10.1080/00405000.2019.1684224.
- [12] E.S. Lee, Innovative Glazing Materials, *Handb. Energy Effic. Build. A Life Cycle Approach*. (2018) 1–23. <https://escholarship.org/content/qt4qj376pk/qt4qj376pk.pdf>.
- [13] Y. Wang, E.L. Runnerstrom, D.J. Milliron, Switchable Materials for Smart Windows, *Annu. Rev. Chem. Biomol. Eng.* 7 (2016) 283–304. doi:10.1146/annurev-chembioeng-080615-034647.
- [14] M. Cipolloni, A. Heynderickx, F. Maurel, A. Perrier, D. Jacquemin, O. Siri, F. Ortica, G. Favaro, Multiswitchable acidichromic and photochromic bisdiarylethene. An experimental and theoretical study, *J. Phys. Chem. C*. 115 (2011) 23096–23106. doi:10.1021/jp205681p.
- [15] L. Wu, S. Zhang, J. Gao, P. Qiang, J. Lei, Preparation of a spirooxazine grafted PMMA and its photochromic properties, *Synth. Commun.* 46 (2016) 818–830. doi:10.1080/00397911.2016.1178296.
- [16] F. Ortica, The role of temperature in the photochromic behaviour, *Dye. Pigment*. 92 (2012) 807–816. doi:10.1016/j.dyepig.2011.04.002.
- [17] C.G. Granqvist, Chapter 13 - Miscellaneous Tungsten- and Molybdenum-Oxide-Containing Films, in: C.G.B.T.-H. of I.E.M. Granqvist (Ed.), Elsevier Science B.V., Amsterdam, 1995: pp. 225–236. doi:<http://dx.doi.org/10.1016/B978-044489930-9/50013-1>.

- [18] Y. Zhong, *Electrochromic Materials and Devices*, Wiley-VCH Verlag GmbH & Co. KGaA, Weinheim, Germany, 2013. doi:10.1002/9783527679850.
- [19] İ.B. Pehlivan, R. Marsal, E. Pehlivan, E.L. Runnerstrom, D.J. Milliron, C.G. Granqvist, G.A. Niklasson, Electrochromic devices with polymer electrolytes functionalized by SiO<sub>2</sub> and In<sub>2</sub>O<sub>3</sub>:Sn nanoparticles: Rapid coloring/bleaching dynamics and strong near-infrared absorption, *Sol. Energy Mater. Sol. Cells.* 126 (2014) 241–247. doi:10.1016/j.solmat.2013.06.010.
- [20] N. Deforest, A. Shehabi, S. Selkowitz, D.J. Milliron, A comparative energy analysis of three electrochromic glazing technologies in commercial and residential buildings, *Appl. Energy.* 192 (2017) 95–109. doi:10.1016/j.apenergy.2017.02.007.
- [21] B.P. Jelle, *Electrochromic Smart Windows for Dynamic Daylight and Solar Energy Control in Buildings*, *Electrochromic Mater. Devices.* (2015) 419–502. doi:10.1002/9783527679850.ch15.
- [22] N.L. Sbar, L. Podbelski, H. Mo, B. Pease, Electrochromic dynamic windows for office buildings, *Int. J. Sustain. Built Environ.* 1 (2012) 125–139. doi:10.1016/j.ijsbe.2012.09.001.
- [23] S. Papaefthimiou, E. Syrrakou, P. Yianoulis, Energy performance assessment of an electrochromic window, *Thin Solid Films.* 502 (2006) 257–264. doi:10.1016/j.tsf.2005.07.294.
- [24] N. DeForest, A. Shehabi, G. Garcia, J. Greenblatt, E. Masanet, E.S. Lee, S. Selkowitz, D.J. Milliron, Regional performance targets for transparent near-infrared switching electrochromic window glazings, *Build. Environ.* 61 (2013) 160–168. doi:10.1016/j.buildenv.2012.12.004.
- [25] A. Cannavale, *Chromogenic Technologies for Energy Saving*, *Clean Technol.* 2 (2020) 462–475. doi:10.3390/cleantechnol2040029.
- [26] A. Piccolo, Thermal performance of an electrochromic smart window tested in an environmental test cell, *Energy Build.* 42 (2010) 1409–1417. doi:10.1016/j.enbuild.2010.03.010.
- [27] A. Piccolo, F. Simone, Performance requirements for electrochromic smart window, *J. Build. Eng.* 3 (2015) 94–103. doi:10.1016/j.jobe.2015.07.002.
- [28] A. Piccolo, C. Marino, A. Nucara, M. Pietrafesa, Energy performance of an electrochromic switchable glazing: Experimental and computational assessments, *Energy Build.* 165 (2018) 390–398. doi:10.1016/j.enbuild.2017.12.049.
- [29] N. DeForest, A. Shehabi, J. O'Donnell, G. Garcia, J. Greenblatt, E.S. Lee, S. Selkowitz, D.J. Milliron, United States energy and CO<sub>2</sub> savings potential from deployment of near-infrared electrochromic window glazings, *Build. Environ.* 89 (2015) 107–117. doi:10.1016/j.buildenv.2015.02.021.
- [30] A. Cannavale, F. Martellotta, P. Cossari, G. Gigli, Energy savings due to building integration of innovative solid-state electrochromic devices, *Appl. Energy.* 225 (2018) 975–985. doi:10.1016/j.apenergy.2018.05.034.
- [31] A. Cannavale, F. Fiorito, D. Resta, G. Gigli, Visual comfort assessment of smart photovoltachromic windows, *Energy Build.* 65 (2013) 137–145. doi:10.1016/j.enbuild.2013.06.019.
- [32] J. Wienold, J. Christoffersen, Evaluation methods and development of a new glare

prediction model for daylight environments with the use of CCD cameras, *Energy Build.* 38 (2006) 743–757. doi:10.1016/j.enbuild.2006.03.017.

- [33] A. Nabil, J. Mardaljevic, Useful daylight illuminances: A replacement for daylight factors, *Energy Build.* 38 (2006) 905–913. doi:10.1016/j.enbuild.2006.03.013.
- [34] A. Nabil, J. Mardaljevic, Useful daylight illuminance: a new paradigm for assessing daylight in buildings, *Light. Res. Technol.* 37 (2005) 41–59. doi:10.1191/1365782805li128oa.
- [35] C.G. Granqvist, İ.B. Pehlivan, G.A. Niklasson, Electrochromics on a roll : Web-coating and lamination for smart windows, *Surf. Coat. Technol.* 336 (2017) 133–138. doi:10.1016/j.surfcoat.2017.08.006.
- [36] M.B. Armand, Polymer Electrolytes, *Annu. Rev. Mater. Sci.* 16 (1986) 245–261. doi:10.1146/annurev.ms.16.080186.001333.
- [37] A.L.-S. Eh, X. Lu, P.S. Lee, Advances in Polymer Electrolytes for Electrochromic Applications, in: *Electrochromic Mater. Devices*, Wiley-VCH Verlag GmbH & Co. KGaA, 2013: pp. 289–310. doi:10.1002/9783527679850.ch10.
- [38] C. Granqvist, *Electrochromic Materials and Devices*, Wiley-VCH Verlag GmbH & Co. KGaA, Weinheim, Germany, 2013. doi:10.1002/9783527679850.
- [39] C.G. Granqvist, Chapter 28 - Devices with Liquid Electrolytes, in: *C.G.B.T.-H. of I.E.M. Granqvist (Ed.), Elsevier Science B.V., Amsterdam, 1995: pp. 459–471.* doi:http://dx.doi.org/10.1016/B978-044489930-9/50028-3.
- [40] V. Di Noto, S. Lavina, G. a. Giffin, E. Negro, B. Scrosati, Polymer electrolytes: Present, past and future, *Electrochim. Acta.* 57 (2011) 4–13. doi:10.1016/j.electacta.2011.08.048.
- [41] C.A. Nguyen, S. Xiong, J. Ma, X. Lu, P.S. Lee, High ionic conductivity P(VDF-TrFE)/PEO blended polymer electrolytes for solid electrochromic devices., *Phys. Chem. Chem. Phys.* 13 (2011) 13319–26. doi:10.1039/c0cp01505a.
- [42] U.O. Krašovec, A. Georg, A. Georg, V. Wittwer, J. Luther, M. Topič, Performance of a solid-state photoelectrochromic device, *Sol. Energy Mater. Sol. Cells.* 84 (2004) 369–380. doi:10.1016/j.solmat.2004.01.043.
- [43] T. Niwa, O. Takai, Optical and electrochemical properties of all-solid-state transmittance-type electrochromic devices, *Thin Solid Films.* 518 (2010) 1722–1727. doi:10.1016/j.tsf.2009.11.062.
- [44] X. Chen, S. Dou, W. Li, D. Liu, Y. Zhang, Y. Zhao, Y. Li, J. Zhao, X. Zhang, All solid state electrochromic devices based on the LiF electrolyte, *Chem. Commun.* 56 (2020) 5018–5021. doi:10.1039/d0cc00697a.
- [45] Y. Zhu, L. Xie, T. Chang, J. Bell, A. Huang, P. Jin, S. Bao, High performance all-solid-state electrochromic device based on  $\text{Li}_x\text{NiO}_y$  layer with gradient Li distribution, *Electrochim. Acta.* 317 (2019) 10–16. doi:10.1016/j.electacta.2019.05.125.
- [46] W. Li, X. Zhang, X. Chen, Y. Zhao, W. Sun, Y. Xiao, S. Li, J. Zhao, Y. Li, Long life all-solid-state electrochromic devices by annealing, *Sol. Energy Mater. Sol. Cells.* 224 (2021) 110992. doi:10.1016/j.solmat.2021.110992.
- [47] K.J. Patel, G.G. Bhatt, J.R. Ray, P. Suryavanshi, C.J. Panchal, All-inorganic solid-state

electrochromic devices: a review, *J. Solid State Electrochem.* 21 (2017) 337–347.  
doi:10.1007/s10008-016-3408-z.

- [48] B.P. Jelle, Electrochromic Smart Windows for Dynamic Daylight and Solar Energy Control in Buildings, in: *Electrochromic Mater. Devices*, Wiley-VCH Verlag GmbH & Co. KGaA, 2013: pp. 419–502. doi:10.1002/9783527679850.ch15.
- [49] C.G. Granqvist, Chapter 8 - Tungsten Oxide Films: Ultraviolet Absorption and Semiconductor Bandgap, in: *C.G.B.T.-H. of I.E.M. Granqvist (Ed.)*, Elsevier Science B.V., Amsterdam, 1995: pp. 139–146. doi:http://dx.doi.org/10.1016/B978-044489930-9/50008-8.